Lecture Notes
in Computational Science
and Engineering 35

Contents

Higher Order Discontinuous Galerkin Methods for Flow and Transport in Porous Media

Peter Bastian

Interdisziplinäres Zentrum für Wissenschaftliches Rechnen, Universität Heidelberg, Im Neuenheimer Feld 348, 69120 Heidelberg, Germany

Summary. In this paper we describe higher order discontinuous Galerkin (DG) methods for application in subsurface transport. Based on a scheme developed by Oden, Babuška and Baumann we present a method for the solution of the elliptic flow equation and describe a multigrid method for the fast solution of the arising algebraic equations. For the solution of the transport equation we combine the DG space discretization with higher order explicit Runge-Kutta schemes in the convection-dominated case and with diagonally implicit Runge-Kutta schemes in the diffusion-dominated case. Numerical results are presented for single-phase flow in heterogeneous media, solute transport and two-phase flow.

1 Introduction

In this paper we are interested in the accurate numerical solution of the equations describing the flow of fluids and dissolved components in the subsurface.

Let Ω be a domain in $\mathbb{R}^d$, $d = 2, 3$, with outward unit normal n. The equation for groundwater flow in head-based formulation is given by

$$\nabla \cdot u = f \quad \text{in } \Omega, \quad u = -K\nabla H, \tag{1}$$

with Dirichlet boundary conditions $H = H_0$ on Γ_H and flux boundary conditions $u \cdot n = U$ on boundary Γ_U. H is the hydraulic head, u is the Darcy velocity and K is the permeability tensor.

The challenge for numerical methods solving (1) is to achieve high accuracy for the flow velocity u subsequently entering the transport equation. Moreover, the permeability tensor may vary over many orders of magnitude.

The generic transport equation including convective and dispersive transport, radioactive decay and a reaction term reads

$$R\Phi\left(\frac{\partial C}{\partial t} + \lambda C\right) + \nabla \cdot j = q(C) \quad \text{in } \Omega, \quad j = uC - D(u)\nabla C \tag{2}$$

Finite Element Methods for Coupled Problems in Ferrohydrodynamics

Olga Lavrova[1], Gunar Matthies[1], Teodora Mitkova[1], Viktor Polevikov[2], and Lutz Tobiska[1]

[1] Institut für Analysis und Numerik, Otto-von-Guericke-Universität Magdeburg, PF4120, 39016 Magdeburg, Germany
[2] Belarusian State University, 4 F. Skaryna Ave., 220050 Minsk, Belarus

Summary. The interaction between a magnetisable fluid and an external magnetic field gives rise to several interesting phenomena in ferrohydrodynamics. Our mathematical models and solution strategies are mainly focused on cases in which the magnetic liquid exhibits a free surface which is not known a-priori. In particular, two special problems are taken into consideration: the behaviour of a ferrofluid drop in a rotary shaft seal and the generation of an ordered pattern of surface protuberances when the applied field exceeds a critical value.

1 Ferrofluids: Properties and Applications

Ferrohydrodynamics (FHD) deals with the mechanics of fluid motion influenced by strong forces of magnetic polarisation. In the well-known discipline of magnetohydrodynamics (MHD) the body force acting on the fluid is the Lorentz force that arises when electric current flows at an angle to the direction of an imposed magnetic field. However, in FHD the fluid is nonconducting and the body force is due to polarisation force. The principal type of a magnetic fluid arising in FHD is a ferrofluid.

Ferrofluids are colloidal suspensions of finely divided ferromagnetic (Fe, Co, Ni) or ferrimagnetic (Fe_3O_4) particles (of size 3-15 nm) in a carrier liquid (water, oil, bio-compatible liquids). In order to avoid agglomeration the monodomain particles are coated with a molecular layer of a dispersant. A schematic representation is shown in Fig. 1 taken from [13]. A colloidal ferrofluid has do be synthesised, since it is not found in nature. A typical ferrofluid contains about 10^{14} particles per cubic millimetre and is photoresist ('black').

If the applied magnetic field is increased then the following states can be observed:

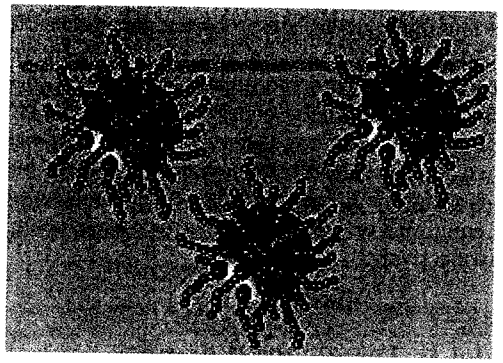

Fig. 1. Magnetic particles with dispersant layer in a ferrofluid

- a random orientation of the particles with no net magnetisation,
- a tendency for alignment, partially overcome by thermal agitation,
- the particles become more and more aligned with the field direction,
- the particles are completely aligned and the magnetisation achieves its saturation value.

The possibility to influence the hydrodynamic parameters of the fluid by an external magnetic field opens the way for a variety of technical and medical applications, like zero-leakage rotary shaft seals, liquid-cooled loudspeakers and magnetic drug targeting. For example, magnetic fluid seals are used to admit both a rotary motion and a hermetic isolation of a high from a low pressure environment. That way sensitive electronical components, like hard disks, can be protected from outside contaminants. In liquid-cooled loudspeakers the lubrication and damping properties can be controlled by the viscosity of the carrier liquid. Further, the heat transfer from the coil can be improved since the thermal conductivity is larger than that of air. In the field of medical drug targeting a magnetic field can pilot the path of a drop of ferrofluid in the body bringing and retaining drugs to a target site. Localised treatment of a disease becomes possible and unwanted side effects can be considerably decreased. For further interesting technical applications of ferrofluids we refer to [3, 18].

The paper is organised as follows. Section 2 is devoted to modelling aspects for describing the interaction between magnetic fields and magnetic fluids. The basic model consists of the incompressible Navier-Stokes equations coupled with the Maxwell equations for a nonconducting fluid. Then, in Sect. 3 the general model is simplified to describe the behaviour of a ferrofluid drop in a rotary shaft seal. We propose a splitting of the coupled nonlinear partial

differential equations into smaller subproblems and discuss their robust and accurate numerical solution. Finally, in Sect. 4, the Rosensweig instability of spontaneous generation of an ordered pattern of surface protuberances when the field exceeds a critical value is considered. In particular two geometric models are discussed which mainly differ in the parametrisation of the unknown free surface. We describe our numerical solution strategies and present numerical tests showing the influence of the used geometric model and different constitutive equations on the shape of surface and the calculated critical magnetic field, respectively.

2 Basic Model in Ferrohydrodynamics

We start with the Maxwell equations for a nonconducting media in the stationary case given by

$$\operatorname{curl} \mathbf{H} = \mathbf{0}, \qquad \operatorname{div} \mathbf{B} = 0 \qquad \text{in } \Omega \ , \tag{1}$$

where $\mathbf{H}$ and $\mathbf{B}$ denote the magnetic field strength and magnetic induction, respectively. The first equation guarantees the existence of a magnetostatic potential. Let us suppose that the ferrofluid occupies the domain Ω_F, with $\overline{\Omega_F} \subset \Omega \subset \mathbb{R}^d$, $d = 2$ or $d = 3$, and that the media outside of Ω_F is nonmagnetisable. Then, we complete (1) by the constitutive relation

$$\mathbf{B} = \begin{cases} \mu_0(\mathbf{M} + \mathbf{H}) & \text{in } \Omega_F \ , \\ \mu_0 \mathbf{H} & \text{in } \Omega \backslash \Omega_F \ , \end{cases} \tag{2}$$

where $\mathbf{M}$ denotes the magnetisation and $\mu_0 = 4\pi \cdot 10^{-7}\mathrm{Vs/Am}$ is the permeability constant. The magnetisation $\mathbf{M}$ of a ferrofluid is parallel to the magnetic field $\mathbf{H}$ and the modulus $M = |\mathbf{M}|$ follows the nonlinear magnetisation law

$$M(H) = M_S \, L(\gamma H) = M_S \left(\coth(\gamma H) - \frac{1}{\gamma H} \right) \tag{3}$$

with $H = |\mathbf{H}|$, the saturation magnetisation M_S, the Langevin function L, the Langevin parameter $\gamma = 3\chi_0 / M_S$, and the initial susceptibility $\chi_0 = \partial_H M(0)$. Consequently, we have

$$\mathbf{M} = M(H) \frac{\mathbf{H}}{H} = \frac{M_S}{H} \left(\coth(\gamma H) - \frac{1}{\gamma H} \right) \mathbf{H} \ . \tag{4}$$

The hydrodynamical properties of the magnetic liquid are described by the time-dependent incompressible Navier-Stokes equations

$$\varrho \, (\mathbf{u}_t + (\mathbf{u} \cdot \nabla)\mathbf{u}) = \operatorname{div} \boldsymbol{\sigma}(\mathbf{u}, p, \mathbf{H}) + \mathbf{f} \qquad \text{in } \Omega_F(t), \ t > 0 \ , \tag{5}$$

$$\operatorname{div} \mathbf{u} = 0 \qquad \text{in } \Omega_F(t), \ t > 0 \ , \tag{6}$$

where $\boldsymbol{\sigma}(\mathbf{u}, p, \mathbf{H})$ is the stress tensor

$$\sigma_{ij}(\mathbf{u}, p, \mathbf{H}) = 2\eta \mathcal{D}(\mathbf{u})_{ij} - \left(p + \frac{\mu_0}{2} H^2 \right) \delta_{ij} + B_i H_j, \qquad i, j = 1, \ldots d \ , \tag{7}$$

consisting of a hydrodynamic and magnetic part. Here, ϱ denote the fluid density, $\mathbf{f}$ the volume force, η the dynamic viscosity, $\mathbf{u}$ the velocity, $p = p_f + p_m$ the (composite) pressure with the thermodynamic pressure p_f in the fluid and the fluid-magnetic pressure

$$p_m = \mu_0 \int_0^H M(H') \, dH' \ , \tag{8}$$

and $\mathcal{D}(\mathbf{u})$ the velocity deformation tensor defined by

$$\mathcal{D}(\mathbf{u})_{ij} = \frac{1}{2} \left(\frac{\partial u_i}{\partial x_j} + \frac{\partial u_j}{\partial x_i} \right), \qquad i, j = 1, \ldots d \ . \tag{9}$$

Using (7) and (9) we can rewrite (5), (6) into

$$\varrho \, (\mathbf{u}_t + (\mathbf{u} \cdot \nabla)\mathbf{u}) - \eta \Delta \mathbf{u} + \nabla \, p = \mathbf{f} + \mu_0 M \nabla H \qquad \text{in } \Omega_F(t), \ t > 0 \ , \tag{10}$$

$$\operatorname{div} \mathbf{u} = 0 \qquad \text{in } \Omega_F(t), \ t > 0 \ . \tag{11}$$

Let us consider the force balance

$$[|\boldsymbol{\sigma} \mathbf{n}|] = \alpha \mathcal{K} \mathbf{n} \qquad \text{on } \Gamma_F(t), \ t > 0 \ , \tag{12}$$

where $\Gamma_F(t)$ is the free surface between a magnetisable medium 1 (ferrofluid) and a nonmagnetisable medium 2 (vacuum, air). Here, $\mathcal{K}$ denote the sum of principal curvatures, $\mathbf{n}$ the unit normal vector, and α the coefficient of surface tension. Multiplying with the unit normal vector we obtain the Young-Laplace equation at the interface $\Gamma_F(t)$

$$-2\eta \mathbf{n} \cdot \mathcal{D}(\mathbf{u}) \mathbf{n} + p_f + p_m + \frac{\mu_0}{2} (\mathbf{M} \cdot \mathbf{n})^2 = p^{(2)} + \alpha \mathcal{K} \tag{13}$$

where $p^{(2)}$ is the pressure in medium 2.

Finally, we add the kinematic condition

$$\mathbf{u} \cdot \mathbf{n} = V_\Gamma, \qquad \text{on } \Gamma_F(t), \ t > 0 \ , \tag{14}$$

with the normal velocity of the free boundary V_Γ. Note that (1)-(3), (10)-(12), (14) are a coupled system of nonlinear partial differential equations with a free boundary $\Gamma_F(t)$, $t > 0$. In the following sections we consider two examples with a time-independent free boundary $\Gamma_F(t) = \Gamma_F$.

3 Rotary Shaft Seals

Let us consider a rotary shaft seal as shown in Fig. 2 where 1 denotes the magnet, 2 the core, 3 the concentrator, 4 the shaft (rotor), and 5 the magnetic fluid bridge. A complete simulation of the behaviour of the ferrofluid drop in the seal would require

- the solution of the Maxwell equations between the rotary shaft and the concentrator in the fluid and the surrounding media,
- the solution of the incompressible Navier-Stokes equations in the fluid,
- the solution of the heat equation in the fluid, shaft, and concentrator.

Furthermore, we have to take into consideration the interface conditions at the free surfaces. Finally, we get a coupled system of nonlinear partial differential equations for the velocity $\mathbf{u}$, the pressure p, the magnetic field strength $\mathbf{H}$, the temperature T, and the positions of the free boundaries.

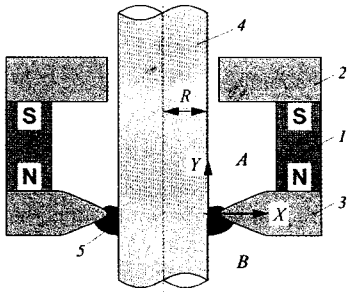

Fig. 2. Rotary shaft seal

3.1 Simplified Model

Under stationary operating conditions the fluid domain can be considered to be rotationally symmetric. Thus, using cylindrical coordinates $x = r\cos\varphi$, $y = r\sin\varphi$, $z = z$ and assuming that the velocity $\mathbf{u} = (u_r, u_\varphi, u_z)$, the thermodynamic pressure p_f and the temperature T depend on r and z only, the incompressible Navier-Stokes equations (10), (11) and the heat equation can be represented in the form

$$\left(u_r\frac{\partial u_r}{\partial r} - \frac{u_\varphi^2}{r} + u_z\frac{\partial u_r}{\partial z}\right) + \frac{\partial p_f}{\partial r} = \nu\left(\frac{\partial^2 u_r}{\partial r^2} + \frac{1}{r}\frac{\partial u_r}{\partial r} - \frac{u_r}{r^2} + \frac{\partial^2 u_r}{\partial z^2}\right) ,$$

$$\left(u_r\frac{\partial u_\varphi}{\partial r} + \frac{u_r u_\varphi}{r} + u_z\frac{\partial u_\varphi}{\partial z}\right) = \nu\left(\frac{\partial^2 u_\varphi}{\partial r^2} + \frac{1}{r}\frac{\partial u_\varphi}{\partial r} - \frac{u_\varphi}{r^2} + \frac{\partial^2 u_\varphi}{\partial z^2}\right) ,$$

$$\left(u_r\frac{\partial u_z}{\partial r} + u_z\frac{\partial u_z}{\partial z}\right) + \frac{\partial p_f}{\partial z} = \nu\left(\frac{\partial^2 u_z}{\partial r^2} + \frac{1}{r}\frac{\partial u_z}{\partial r} + \frac{\partial^2 u_z}{\partial z^2}\right) ,$$

$$\left(\frac{\partial u_r}{\partial r} + \frac{1}{r}u_r + \frac{\partial u_z}{\partial z}\right) = 0 ,$$

$$u_r\frac{\partial T}{\partial r} + u_z\frac{\partial T}{\partial z} - \frac{\nu}{c_p}\Phi(\mathbf{u}) = \lambda\left(\frac{\partial^2 T}{\partial r^2} + \frac{1}{r}\frac{\partial T}{\partial r} + \frac{\partial^2 T}{\partial z^2}\right) .$$

Here, the gravitational force has been neglected in the momentum equation and λ denotes the thermal conduction, c_p the specific heat, $\nu = \eta/\varrho$ the kinematic viscosity, and Φ is the dissipation function given by

$$\Phi(\mathbf{u}) = 2\left[\left(\frac{\partial u_r}{\partial r}\right)^2 + \left(\frac{1}{r}u_r\right)^2 + \left(\frac{\partial u_z}{\partial z}\right)^2\right] + \left(\frac{\partial u_r}{\partial z} + \frac{\partial u_z}{\partial r}\right)^2 + \left(\frac{\partial u_\varphi}{\partial z}\right)^2 + \left(\frac{\partial u_\varphi}{\partial r} - \frac{1}{r}u_\varphi\right)^2 .$$

Let R be the radius of the rotor, $a \ll R$ the gap width, u_0 the circumferential velocity of the rotor at $r = R$, and T_0 the characteristic temperature. We introduce dimensionless variables

$$X = \frac{r-R}{a},\ Y = \frac{z}{a},\ v_1 = \frac{u_r}{u_0},\ v_2 = \frac{u_z}{u_0},\ w = \frac{u_\varphi}{u_0},\ p = \frac{p_f}{\varrho u_0^2},\ \vartheta = \frac{T}{T_0}$$

and approximate the term representing centrifugal forces in the momentum equation

$$-\frac{u_\varphi^2}{r} = -\frac{u_0^2}{a}\,\frac{a}{R+aX}\,w^2 = -\frac{u_0^2}{a}\,\frac{\delta}{1+\delta X}\,w^2 \approx -\frac{u_0^2}{a}\,\delta\,w^2$$

by taking into consideration that the relative width of the gap $\delta = a/R \ll 1$. All other terms with the factor

$$\frac{a}{r} = \frac{a}{R+aX} = \frac{\delta}{1+\delta X} \ll 1$$

are neglected. That way we end up with a problem for the azimuthal velocity w, the secondary flow $\mathbf{v} = (v_1, v_2)$, the pressure p, and the temperature ϑ in the cross-section $\Omega_F \subset \mathbb{R}^2$:

$$-\frac{1}{\mathrm{Re}}\Delta w + \mathbf{v}\cdot\nabla w = 0 \qquad \text{in } \Omega_F\ , \qquad (15)$$

$$-\frac{1}{\mathrm{Re}}\Delta \mathbf{v} + \mathbf{v}\cdot\nabla\mathbf{v} + \nabla p = \delta\, w^2\, \mathbf{e}_X \qquad \text{in } \Omega_F\ , \qquad (16)$$

$$\nabla\cdot\mathbf{v} = 0 \qquad \text{in } \Omega_F\ , \qquad (17)$$

$$-\frac{1}{\mathrm{Pr}\ \mathrm{Re}}\Delta\vartheta + \mathbf{v}\cdot\nabla\vartheta = \frac{\Lambda}{\mathrm{Re}}\frac{a^2}{u_0^2}\Phi(\mathbf{u}) \qquad \text{in } \Omega_F\ . \qquad (18)$$

Here, we have used the notations $\mathrm{Re} = u_0 a/\nu$ for the Reynolds number, $\mathrm{Pr} = \nu/\lambda$ for the Prandtl number, $\mathbf{e}_X$ for the unit vector in the X-direction, and $\Lambda = u_0^2/c_p T_0$.

The derivation of weak formulations of (15)-(17) can be found in [12], where also the solvability of the problem is analysed. Both existence and uniqueness (for small δ) of the weak solution follow from the general theory of saddle point problems, the standard Galerkin method and a weak maximum principle.

We can achieve a further simplification by taking into consideration that the magnitude of the azimuthal velocity w is much larger than the secondary flow $\mathbf{v}$. Under this assumption we can neglect $\mathbf{v}\cdot\nabla w \approx 0$ in (15) and use the simpler form of the dimensionless dissipation function

$$\frac{a^2}{u_0^2}\Phi(\mathbf{u}) \approx \tilde{\Phi}(w) = \left(\frac{\partial w}{\partial X}\right)^2 + \left(\frac{\partial w}{\partial Y}\right)^2$$

in (18). Thus, given the azimuthal velocity we can determine the secondary flow and the temperature by solving the two-dimensional problem (16)-(18).

Let us consider the case of a hyperbolic concentrator shape and assume that the permeability of the shaft and concentrator is much higher than the permeability of the fluid. Moreover, let $M \ll H$ which implies that the shape of the free surface has practically no influence on the local magnetic field strength. Under these assumptions we are able to give an explicit analytical expression for the magnetic field strength by transforming the domain between the shaft and the concentrator onto an infinite strip [17].

Concerning the Young-Laplace equation we neglect the influence of gravity, surface tension, the magnetic normal pressure $(\mathbf{M}\cdot\mathbf{n})^2\mu_0/2$, and the flow on the free surface (cf. [17]). Thus, (13) reduces finally to the balance $p_f + p_m = p^{(2)}$ of fluid and fluid-magnetic pressure with the outer pressure $p^{(2)}$ at the free surface. Since in our case $M(H) \approx M_S$ we have $p_m \approx \mu_0 M_S H$. The fluid pressure p_f can be approximated up to a constant by integrating the approximated momentum equation

$$\nabla p \approx \delta\, w^2\, \mathbf{e}_X\ .$$

The constant can be calculated from the condition that the volume of fluid enclosed by the two arcs of free surfaces is given. Together with the analytical

expression for the magnetic field strength the coupled problem for determing the azimuthal velocity w and the shape of the two arcs consists of a boundary value problem for a linear elliptic equation and algebraic equations for the free surfaces [17].

3.2 Solution Strategy

Our simplified model admits the solution strategy shown in Fig. 3.

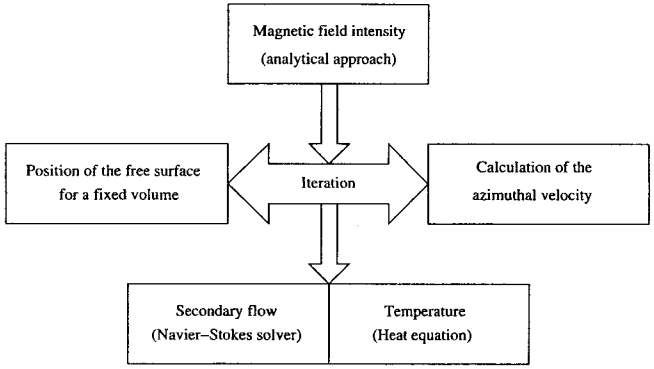

Fig. 3. Iterative decoupling strategy

We start with the analytical expression for the magnetic field and a given cross-section of the fluid domain Ω_F^0. Next, we use an inner iteration to determine w and the free surfaces Γ_F. To this end we calculate the solution of the elliptic equation

$$-\Delta w^k = 0 \quad \text{in } \Omega_F^{k-1}$$

subjected to the boundary conditions

$$w^k = 0 \ \text{ on } \Gamma_C^{k-1}, \quad w^k = 1 \ \text{ on } \Gamma_S^{k-1}, \quad \frac{\partial w^k}{\partial n} = 0 \ \text{ on } \Gamma_F^{k-1}\ ,$$

where the closed contour $\partial\Omega_F^{k-1} = \Gamma_C^{k-1} \cup \Gamma_S^{k-1} \cup \Gamma_F^{k-1}$ consists of the axial cross section of the solid (concentrator and shaft) and free surfaces. Then, to find the new update of the free surfaces $Y_i^k = Y_i^k(X)$, $i = 1, 2$ we solve algebraic equations of the form

$$\mu_0 M_s H(X, Y_i^k(X)) = p_i^{(2)} - p_f(w)(X, Y_i^{k-1}), \quad i = 1, 2\ ,$$

subjected to a fixed volume between the two arcs. The two arcs $(X, Y_i^k(X))$ define the new fluid domain Ω_F^k. We set $k = k + 1$ and repeat the iteration

unless the changes between Ω_F^{k-1} and Ω_F^k are small. Finally, for the results of this iteration w and Ω_F the secondary flow $\mathbf{v}$ and the temperature field ϑ are calculated from (16)-(18).

3.3 Numerical Results

For details on the calculation of the azimuthal velocity w and the free surfaces Γ_F see [17]. We calculate the secondary flow $\mathbf{v}$ and the temperature field ϑ in a fixed domain Ω_F for a given azimuthal velocity w.

In our case the boundary $\partial\Omega_F = \Gamma_F \cup \Gamma_C \cup \Gamma_S$ consist of two free surfaces Γ_F, the boundary of the concentrator Γ_C and of the shaft Γ_S (Fig. 4 shows schematically the geometry of the domain Ω_F). We apply for completing (16)-(18) the following boundary conditions:

$$\mathbf{v} \cdot \mathbf{n} = 0 \quad \text{on} \quad \Gamma_F \ , \tag{19}$$

$$\mathbf{n} \cdot [|\widetilde{\sigma}(\mathbf{v}, p, \mathbf{H})|] \cdot \tau = 0 \quad \text{on} \quad \Gamma_F \, , i, j = 1, 2 \ , \tag{20}$$

$$\mathbf{v} = 0 \quad \text{on} \quad \Gamma_C \cup \Gamma_S \ , \tag{21}$$

$$\vartheta = \vartheta_0 \quad \text{on} \quad \partial\Omega_F \ . \tag{22}$$

Here, τ is the unit tangential vector and $\widetilde{\sigma}(\mathbf{v}, p, \mathbf{H})$ denotes the dimensionless stress tensor. It is important to note that in (20) the magnetic part of the stress tensor does not play any role since the jumps of $\mathbf{H} \cdot \tau$ and $\mathbf{B} \cdot \mathbf{n}$ vanish. Consequently, a slip boundary condition (19) and a condition on the tangential stresses (20) are imposed on the free boundary Γ_F whereas a Dirichlet (or no-slip) boundary condition (21) is prescribed for $\mathbf{u}$ on the remaining part $\partial\Omega_F \backslash \Gamma_F = \Gamma_C \cup \Gamma_S$. The slip and no-slip boundary condition describe different physical situations. This is also reflected in the mathematical treatment of the problem and of the finite element discretisation.

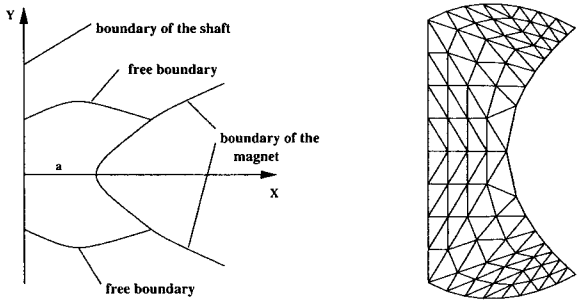

Fig. 4. Geometry of the fluid domain Ω_F (left) and the triangulation for refinement level 2 (right)

All results which we present here were obtained by using the conforming P_2/P_1 finite element pair, i.e., the velocity and the temperature are approximated by continuous, piecewise quadratic functions while the pressure is approximated by continuous, piecewise linear functions. The conforming finite element pair P_2/P_1 satisfies the Babuška-Brezzi stability condition [7], which guarantees a stable discretisation of the saddle point problem (16)-(17). We consider a discretisation where the slip boundary condition (19) is incorporated in the ansatz and the finite element space. It is possible to treat the slip boundary condition (19) as a Lagrange multiplier, see e.g. [2]. Numerically, however, our treatment of the slip boundary condition is less complicated and cheaper.

The discretisation of (16)-(18) corresponds to a linear algebraic system of equations for (18) and a nonlinear algebraic system for the saddle-point problem (16)-(17). The nonlinearity within the problem (16)-(17) is resolved by using a fixed-point iteration (linearisation of the convective term). The nonlinear fixed-point iteration is stopped if the l_2-norm of the residual is less than 10^{-8}. Thus, it remains to solve efficiently a large linear systems in each nonlinear iteration step. We use the geometric multigrid method as an efficient solver. For a detailed discussion of the design of multigrid methods and their efficiency we refer to [8]. The triangulation of the refinement multigrid level 2 is shown in Fig. 4. All finer meshes are constructed by uniform refinement and boundary adaption.

Within the multigrid method for solving the saddle-point problem (16)-(17) we use a V-cycle with one pre-smoothing and one post-smoothing step. As a smoother, we use the block Gauss-Seidel method (Vanka-type smoother, see [20]). The solution of a linear problem (obtained from the linearisation of the convective term) is stopped after a residual reduction of a factor 1/10 or the residual is smaller than 10^{-10}.

The linear algebraic system corresponding to the discretisation of (18) is solved also by applying a geometric multilevel approach. As a smoother on the coarsest level we consider the ILU method while the Jacobi methods is applied on all finer levels. For details see [19]. The stopping criterion is the same as above.

As a testexample we consider a rotary shaft seal with a minimum gap width $a = 1$ and a concrete geometry, which is presented in Fig. 4. We carried out calculations for ferrofluid EMG 905 (for more details on the physical parameters of ferrofluids see [1, 18]. We obtain Re = 63.2456, Pr = 0.7, $\delta = 0.01$, $\Lambda = 1.2295$ as dimensionless parameters. The temperature ϑ_0 on the boundary is given as the room temperature ($\vartheta_0 = 20$). All presented numerical results we have obtained using MooNMD [9].

Table 1 gives the number of cells and degrees of freedom for the P_2/P_1 pair on the different refinement levels. Since we consider a two-dimensional problem the number of unknowns increases by a factor of about 4 from one level to next finer level.

Table 1. Number of degrees of freedom in each level

Level	2	3	4	5	6	7
number of cells	32	128	512	2048	8192	32768
velocity	170	594	2210	8514	33410	132354
pressure	27	85	297	1105	4257	16705
temperature	85	297	1105	4257	16705	66177

Fig. 5 shows that the multigrid method is an efficient solver with respect to the computing times. The computing time to determine the secondary flow increases like $\mathcal{O}(N)$ with the number N of degrees of freedom.

The computed streamlines of the secondary flow on the level 5 and level 7 are visualised in Fig. 6. Figure 7 illustrates the isolines of the temperature on level 5 and level 7. Considering finer triangulations we obtain really reliable results.

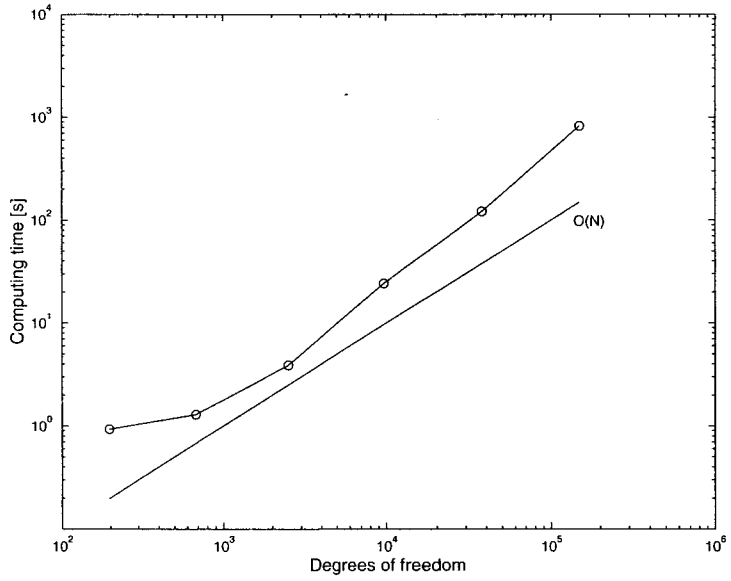

Fig. 5. Computing times (in sec.) to determine the secondary flow for different refinement levels

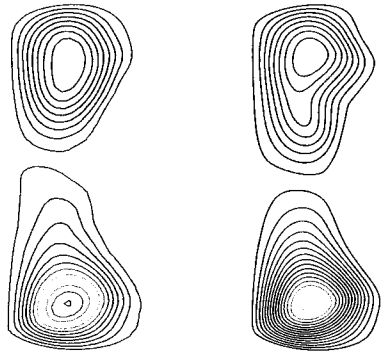

Fig. 6. Streamlines of the secondary flow on level 5 (left) and level 7(right)

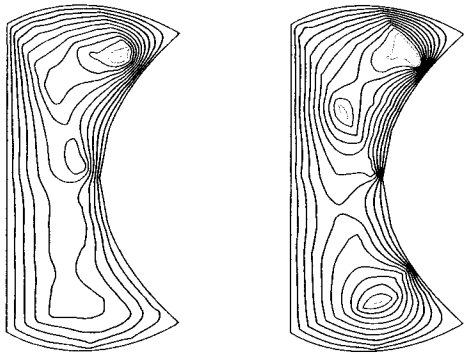

Fig. 7. Isolines of the temperature on level 5 (left) and level 7(right)

4 Rosensweig Instability

4.1 Physical Observation

A perpendicular, uniform magnetic field applied to a layer of ferrofluid generates a spontaneous surface deformation if the field strength exceeds a critical value. This stationary wave pattern on the surface was first observed by Cowley and Rosensweig [4]. This surface instability is caused by the interaction of gravitational, capillary and magnetic forces.

First we will describe in detail a physical experiment which demonstrates the behaviour of a ferrofluid layer in the Rosensweig instability. We start with an undisturbed and flat surface. For small value of the magnetic field strength the interface between ferrofluid and surrounding air remains flat. At a certain

threshold value H_C of the strength of the external applied field the ferrofluid surface deforms into a regular hexagonal pattern and peaks occur. The wave length λ_C of the pattern and the threshold value H_C can be determined by the physical parameters of the ferrofluid. A further increase of the magnetic field strength causes higher peaks. Now we decrease the magnetic field strength. This results in a decreased peak height. Due to a hysteresis the pattern of peaks will exist even if the magnetic field strength H is smaller than the threshold value H_C. If the field is decreased further then the peaks collapse at a second critical value.

4.2 Adaption of the general model to the Rosensweig instability

We consider a horizontally unbounded ferrofluid layer of infinite depth. Figure 8 displays a two-dimensional cut through the three-dimensional surface pattern and a top view of the hexagonal pattern. Furthermore, the critical

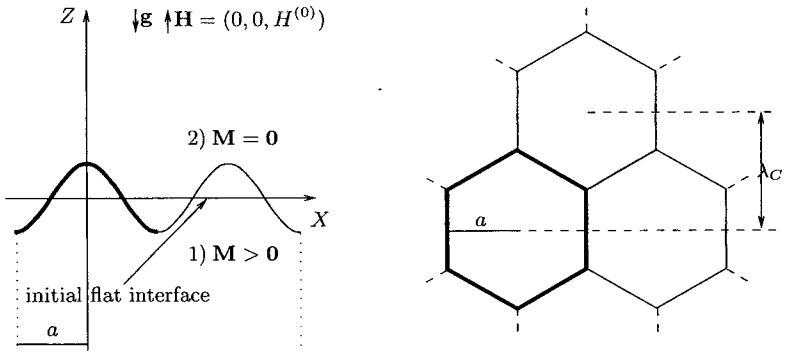

Fig. 8. Illustration of surface deformation, two-dimensional cut (left) and top view with hexagonal structure (right)

wave length λ_C is shown. The value of λ_C can be obtained by

$$\lambda_C = 2\pi\sqrt{\frac{\alpha}{\varrho g}} \ ,$$

see [18]. The critical magnetic field $H_C^{(1)}$ inside the fluid can be calculated from the nonlinear equations

$$M^2(H_C^{(1)}) = \frac{2}{\mu_0}\left(1 + \frac{1}{r_0\left(H_C^{(1)}\right)}\right)\sqrt{\varrho g \alpha}$$

with

$$r_0\left(H_C^{(1)}\right) = \frac{1}{\mu_0}\sqrt{\mu_c\left(H_C^{(1)}\right)\mu_t\left(H_C^{(1)}\right)}$$

and

$$\mu_c\left(H_C^{(1)}\right) = \frac{B^{(1)}\left(H_C^{(1)}\right)}{H_C^{(1)}}, \qquad \mu_t\left(H_C^{(1)}\right) = \frac{\partial B^{(1)}}{\partial H}\left(H_C^{(1)}\right) \ .$$

The critical value $H_C^{(2)}$ for the outer applied field is given by

$$H_C^{(2)} = H_C^{(1)} + M\left(H_C^{(1)}\right) \ ,$$

see [18].

Since the surface protuberances form a regular pattern we restrict our considerations to a domain which is bounded in both horizontal directions, i.e., we consider $\Omega = \Omega' \times \mathbb{R}$ with a bounded domain $\Omega' \in \mathbb{R}^2$. The magnetostatic problem (1)-(2) can be written by using the magnetostatic potential φ as

$$-\mathrm{div}\left(\mu(x, |\nabla\varphi|)\nabla\varphi\right) = 0 \qquad \text{in } \Omega \ , \tag{23}$$

where

$$\mu(x, |\nabla\varphi|) = \begin{cases} \mu_0 & x \in \Omega \setminus \Omega_F \ , \\ \mu_0\left(\frac{M(|\nabla\varphi|)}{|\nabla\varphi|} + 1\right) & x \in \Omega_F \ . \end{cases}$$

In order to apply boundary conditions for the magnetostatic problem we restrict the z-coordinate to the interval $(-Z, Z)$, i.e., we consider the magnetostatic problem in the bounded domain $\Omega' \times (-Z, Z)$. At the bottom and the top boundary we use

$$\varphi = \begin{cases} -ZH^{(1)} & \text{on } \Omega' \times \{-Z\} \\ ZH^{(2)} & \text{on } \Omega' \times \{Z\} \end{cases} \tag{24}$$

as boundary conditions where $H^{(1)}$ and $H^{(2)}$ are the magnetic field strength for the case of an undisturbed interface inside and outside the ferrofluid, respectively. Using this boundary conditions makes sense since we assume that the magnetic field far away from the interface coincide with the field for the case of an undisturbed, flat interface. Due to the regularity of the surface pattern it is reasonable to apply

$$\frac{\partial\varphi}{\partial n} = 0 \qquad \text{on } \partial\Omega' \times (-Z, Z) \ . \tag{25}$$

For the Navier–Stokes equations (10) and (11) we assume that the ferrofluid is at rest, i.e., $\mathbf{u} = \mathbf{0}$. If we take only the gravity as acting force $\mathbf{f}$ in (10) we get

$$\nabla p = -\varrho\mathbf{g} + \mu_0 M \nabla H$$

and obtain

$$p_f + p_m = -\varrho g z + \mu_0 \int_0^H M(H')\, dH' \ .$$

Taking this we get the Young–Laplace equation (13) in the form

$$p^{(2)} + \alpha \mathcal{K} = -\varrho g z + \mu_0 \int_0^H M(H')\, dH' + \frac{\mu_0}{2}(\mathbf{M}\cdot\mathbf{n})^2 + C \qquad (26)$$

where the constant C will be fixed by using a volume constraint.

4.3 Decoupling Strategy

The problem is a coupled system of nonlinear partial differential equations which is splitted into two subproblems. The first one is the magnetostatic problem in a given domain and the second one is the Young–Laplace equation for a given magnetic field. By using a parametrisation of the unknown interface we have a representation of the curvature $\mathcal{K}$ in terms of the unknowns of the interface parametrisation.

For solving the whole system we apply the following decoupling strategy.

S1. Construct an initial mesh for the two-dimensional interface.

S2. Generate a three-dimensional mesh for the magnetostatic potential from the two-dimensional interface mesh.

S3. Solve the magnetostatic problem for a given interface position.

S4. Calculate the unknowns of the surface parametrisation from the Young–Laplace equation using the magnetic field obtained in S3 and get the new interface mesh.

S5. If the norm of the surface change within one iteration is greater than a prescribed threshold then continue with S2 otherwise STOP.

The step S1 has to provided an initial surface. This can be for instance a surface which is slightly disturbed flat interface or a computed surface for a parameter set close to the new one.

4.4 Magnetostatic problem

The magnetostatic problem is nonlinear due to the nonlinearity of the permeability function μ. For solving this problem we apply a fixed-point iteration, i.e., we solve

$$-\mathrm{div}\,(\mu(x, |\nabla\varphi^{k-1}|)\nabla\varphi^k) = 0, \qquad k \geq 1 \ ,$$

with the boundary conditions (24) and (25). In the very first calculation for obtaining φ^1 we start with a magnetic field which corresponds to the case of the undisturbed interface. The magnetostatic problem is uniformly elliptic and has slightly jumping coefficients.

4.5 Parametric free surface equations

We suppose that Γ_F can be considered as a surface of revolution and formulate the problem in the cylindrical coordinates R, Z so that $Z = 0$ is the equation of the unperturbed plane surface. The equilibrium shape is described by the parametric functions $R = R(S)$, $Z = Z(S)$, where S is the arc length of the unknown equilibrium line, $S = 0$ at the peak top on the OZ axis, $S = \ell$ at the peak foot where $R = a$ is the radius of the circle Ω'.

The surface curvature is calculated by the formula $\mathcal{K} = -\left(RZ'\right)' / \left(RR'\right)$ and can be written as $\mathcal{K} = -Z''/R' - Z'/R = R''/Z' - Z'/R$ according to the natural property $(Z')^2 + (R')^2 \equiv 1$ of such a type of parametrisation.

We will use the Vislovich approximation of the magnetisation law [3]

$$M(H) \approx M_S H/(H + H_T)$$

where H_T is the magnetic field strength at which the magnetisation of the fluid is equal to $M_S/2$.

The Young-Laplace equation (26) in axisymmetrical case has the form

$$z'' = r'(f + C), \quad r'' = -z'(f + C); \quad 0 < s < L = \ell/a \ , \qquad (27)$$
$$f = \lambda^2 z - \frac{2\lambda Si}{\chi}(H - \ln(1 + H)) - \lambda Si\left(\frac{\mathbf{H}\cdot\mathbf{n}}{1+H}\right)^2 - z'/r \ ,$$

where $r = R/a$, $z = Z/a$, $s = S/a$ are the dimensionless variables, C the unknown constant, $\lambda = a\sqrt{\rho g/\alpha}$, $Si = \mu_0 M_S^2/(2\sqrt{\rho g \alpha})$, $\chi = M_S/H_T$, and H the field in the magnetic fluid dimensionless on H_T.

Boundary conditions follow from the shape symmetry which in dimensionless formulation take the form

$$r(0) = z'(0) = z'(L) = 0, \quad r(L) = r'(0) = r'(L) = 1 \ , \qquad (28)$$

and are supplemented by the condition of volume conservation

$$\int_0^L zrr'\, ds = 0 \ . \qquad (29)$$

We reformulate the problem (27)-(29) in new dimensionless variables $\tilde{s} = s/L, \tilde{r} = r/L, \tilde{z} = z/L$, what allows us to make computation on a fixed domain $(0, 1)$. Then we construct a second order difference scheme for this problem on a uniform grid and solve the corresponding nonlinear difference problem by an iterative method elaborated in [15, 16].

4.6 Surface as a graph

In this section we abandon the assumption that the free surface can be considered as a revolution surface. We will consider the hexagonal surface pattern

and choose a hexagon as domain Ω'. Furthermore, we assume that the interface Γ_F is given as a graph of a function z, i.e.,

$$\Gamma_F = \{(x_1, x_2, z) \,:\, z = z(x_1, x_2),\ (x_1, x_2) \in \Omega'\} \ .$$

Then, the curvature $\mathcal{K}$ is given by

$$\mathcal{K} = -\mathrm{div}\, \frac{\nabla z}{\sqrt{1 + |\nabla z|^2}} \ .$$

Using a characteristic length A and the strength $H^{(0)}$ of the outer applied field to translate the Young-Laplace equation (26) into dimensionless quantities we obtain after multiply (26) by A/α the following equation

$$-\mathrm{div}\, \frac{\nabla z}{\sqrt{1 + |\nabla z|^2}} + \Lambda^2 z = \Lambda Si \ln\left(\frac{\sinh(\gamma H)}{\gamma H}\right) + \frac{3\chi_0 \Lambda Si}{2} L^2(\gamma H) \left(\frac{\mathbf{H}\cdot\mathbf{n}}{H}\right)^2 + C \tag{30}$$

with the dimensionless parameters

$$\Lambda = A\sqrt{\frac{\varrho g}{\alpha}}, \qquad Si = \frac{\mu_0 M_S^2}{3\chi_0\sqrt{\varrho g \alpha}}, \qquad \gamma = \frac{3\chi_0 H^{(0)}}{M_S}, \qquad \chi_0 = \frac{\partial M}{\partial H}(0) \ .$$

Due to the symmetry of the surface pattern we equip this equation with homogeneous Neumann boundary conditions.

Let F contain all forces on the right-hand side of (30). In the following, we will consider a slightly more general problem in which Λ is not longer a positive constant but a uniformly positive and bounded function on Ω', i.e., $\Lambda \in L^\infty(\Omega')$ and $\Lambda(x_1, x_2) \geq \Lambda_0 > 0$ for $(x, y) \in \Omega'$. This means that we consider the problem

$$-\mathrm{div}\, \frac{\nabla z}{\sqrt{1 + |\nabla z|^2}} + \Lambda^2 z = F \qquad \text{in } \Omega' \ , \tag{31}$$

$$\frac{\partial z}{\partial n} = 0 \qquad \text{on } \partial\Omega' \ . \tag{32}$$

This equation is elliptic but not uniformly elliptic. Moreover, it is nonlinear. We solve this problem by a fixed-point iteration, i.e., we solve the equation

$$-\mathrm{div}\, \frac{\nabla z^k}{\sqrt{1 + |\nabla z^{k-1}|^2}} + \Lambda^2 z^k = F \qquad \text{in } \Omega', \qquad k \geq 1 \ ,$$

with homogenous Neumann boundary conditions on $\partial\Omega'$. As initial guess z^0 we choose the interface position which was used during the calculation of the magnetostatic potential.

Since we want to solve the Young–Laplace equation (31) by a finite element method we have to derive a weak formulation of (31). In order to do so we multiply (31) by a test function $v \in H^1(\Omega')$ and integrate over Ω'. After an integration by parts of the first term we obtain as a weak formulation

Find $z \in H^1(\Omega')$ such that

$$\int_{\Omega'} \frac{\nabla z}{\sqrt{1 + |\nabla z|^2}} \cdot \nabla v \, dx + \int_{\Omega'} \Lambda^2 \, zv \, dx = \int_{\Omega'} Fv \, dx \qquad \forall v \in H^1(\Omega') \ . \tag{33}$$

In the following we assume that the problem (33) has a unique solution z which satisfies $z \in W^{1,\infty}(\Omega')$.

Let $V_h \subset H^1(\Omega')$ an arbitrary finite element space. The discretisation of (33) is given by

Find $z_h \in V_h$ such that

$$\int_{\Omega'} \frac{\nabla z_h}{\sqrt{1 + |\nabla z_h|^2}} \cdot \nabla v_h \, dx + \int_{\Omega'} \Lambda^2 \, z_h v_h \, dx = \int_{\Omega'} F v_h \, dx \qquad \forall v_h \in V_h \ . \tag{34}$$

Now we will estimate the error between the solutions z and z_h of (33) and (34), respectively. As usual in finite element analysis we get an error estimate which is bounded by the interpolation error only.

Theorem 1 (Abstract error estimate). *Let z and z_h be the solutions of (33) and (34), respectively. Furthermore, we assume that $z \in W^{1,\infty}(\Omega')$. Then we get*

$$\frac{K(z)}{2}\Theta^2 + \frac{3}{4}\Lambda_0^2 \|z - z_h\|_{0,2,\Omega'}^2 \leq C(z) \inf_{v_h \in V_h} \|z - v_h\|_{1,2,\Omega'}^2 \tag{35}$$

where

$$\Theta := \left(\int_{\Omega'} \frac{|\nabla(z - z_h)|^2}{\sqrt{1 + |\nabla z_h|^2}} \, dx\right)^{1/2} \ .$$

The quantities $C(z)$ and $K(z)$ are positive constants which are independent of V_h.

The statement of the previous theorem leads together with standard approximation results for finite element spaces to the following corollary.

Corollary 1 (Error estimates). *Let $z \in H^{k+1}(\Omega') \cap W^{1,\infty}(\Omega')$ be the solution of (33). The space V_h consists of finite elements of order k. Then we have*

$$\|z - z_h\|_{0,2,\Omega'} \leq C(z)\, h^k, \qquad \text{and} \qquad |z - z_h|_{1,2,\Omega'} \leq C(z)\, h^k \ ,$$

where the constant $C(z)$ depends only on z but not on h.

The proof of Theorem 1 and Corollary 1 can be found in [10].

4.7 Numerical Results

Calculated peak shapes.

As a first result we will show in Fig. 9 the peak shapes which we have obtained by the method describe in Sect. 4.6 using MooNMD [9]. As expected, the

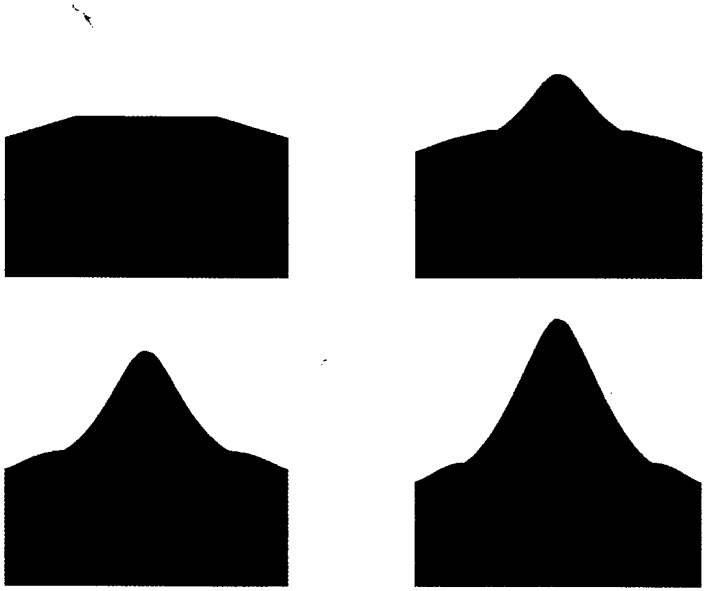

Fig. 9. Peak shape for different applied fields

interface remains flat if the outer applied field doesn't exceed the critical threshold (upper left subplot). If the applied field is larger than the critical value H_C then we obtain a peak (upper right). The lower row in Fig. 9 shows that an increasing magnetic field will lead to an increased peak height.

Hysteresis.

Ferrofluids show an hysteretic behaviour if the magnetic field strength is decreased from a supercritical value to a subcritical value. Figure 10 shows the peak height for the ferrofluid APG 512A. The marker o indicates the path with an increasing field while the marker $*$ labels the path of a decreasing

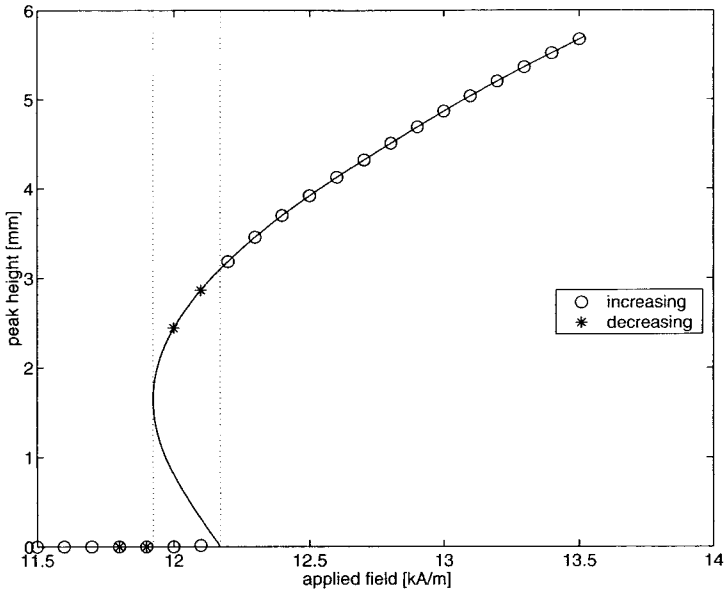

Fig. 10. Hysteresis for ferrofluid APG 512A together with a fit

field. There is a region for the magnetic field strength, between the two vertical lines in Fig. 10, below the critical value where two surface shapes are possible, a flat interface or a developed peak. Which shape occurs in the experiment depends on the way in which the applied field strength was achieved. If the magnetic field strength is increased from a lower value then the surface remains flat. If the magnetic field strength is decreased from a value above the critical value then a pattern of peaks is obtained. A classical result for the dependence of the peak height on the strength of the applied field can be found in [6] where the magnetisation M was approximated by $M = \chi H$ with a constant susceptibility χ. Recently, the pattern and wavenumber selection in ferrofluid layers of finite and infinite depth was investigated in [5]. The physical theory predicts that the dimensionless quantity

$$\varepsilon = \frac{H^2 - H_C^2}{H_C^2}$$

is a polynomial in dimensionless peak height h. Figure 10 shows a fit with a polynomial of degree 6 through the data which were obtained by our simulations. The agreement between the fit and the data is quite good.

Comparison between the models from Sect. 4.5 and 4.6.

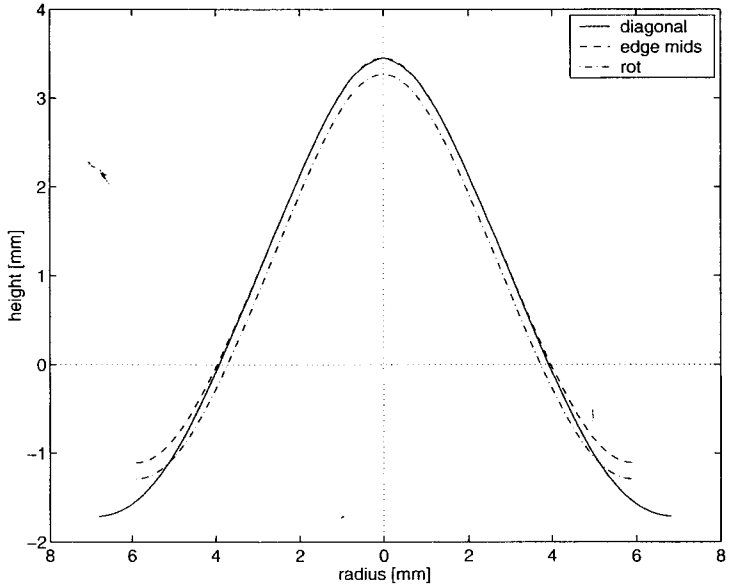

Fig. 11. Cuts through a peak along diagonal, line connecting midpoints of two opposite edges, and shape obtained by the parametric surface model

The following results were obtained for the ferrofluid EMG 909. Figure 11 shows the peak shape obtained by the parametric surface model and two cuts through a peak obtained by the graph model. One cut goes along a diagonal from one vertex to the opposite one. The second cut connects the midpoints of two opposite edges of the hexagon. We see that for the centre of the peak the assumption of rotational symmetry is reasonable. The difference occur only in the regions which have a greater distance from the middle of the peak. The results from the calculation with assumed rotational symmetry produces a peak which is a little bit smaller but the shape is very similar to that obtained by the fully three-dimensional calculations.

Now we will investigate how the assumption of rotational symmetry influences the peak height and the value for the critical field. Figure 12 shows the peak top and foot z-coordinates in dependence on the outer applied field. We see that the calculations which were made with the assumption of rotational symmetry produces peaks which are smaller than those obtained by the fully 3d model. Note that for both cases the Vislovich approximation was used which

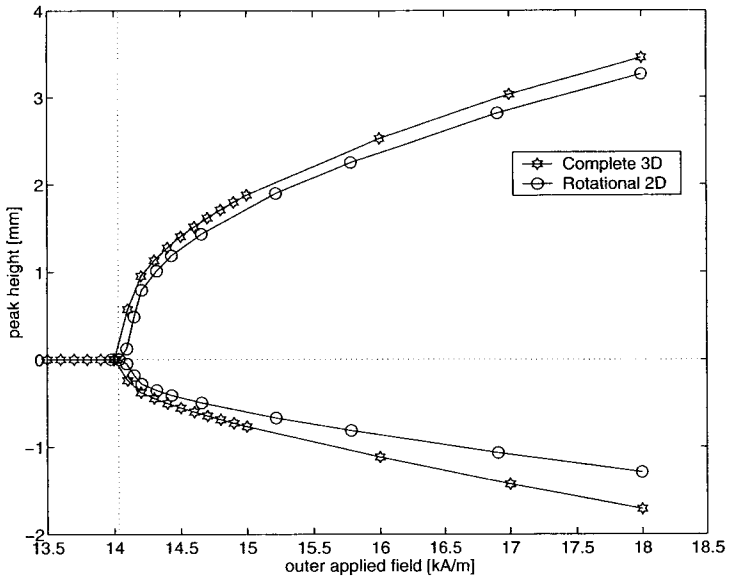

Fig. 12. Comparison of rotational symmetric and complete 3d calculation

results in a theoretical value $H_C = 14.03$ kA/m for the critical magnetic field strength. This value is shown in Fig. 12 as a vertical line. The fully 3d calculations produce, compared to the 2d rotational calculations, a value for the critical magnetic field strength which is closer to the theoretical one.

Comparison of different magnetisation laws in the 3d model.

Now we will consider the influence of the used constitutive equation on the peak height. We compare calculations with the model describe in Sect. 4.6 for the Langevin function and its Vislovich approximation. Due to the different magnetisation laws we obtain also different values for the critical magnetic field H_C. For the Langevin function this value is given by 14.85 kA/m while the Vislovich approximation results in a value of 14.03 kA/m. Both values are given in Fig. 13 as vertical lines. Figure 13 shows that both critical values are reproduced very well by the finite element approximation. Furthermore, we see that the peak height for the Langevin function increases more rapidly compared to the Vislovich approximation.

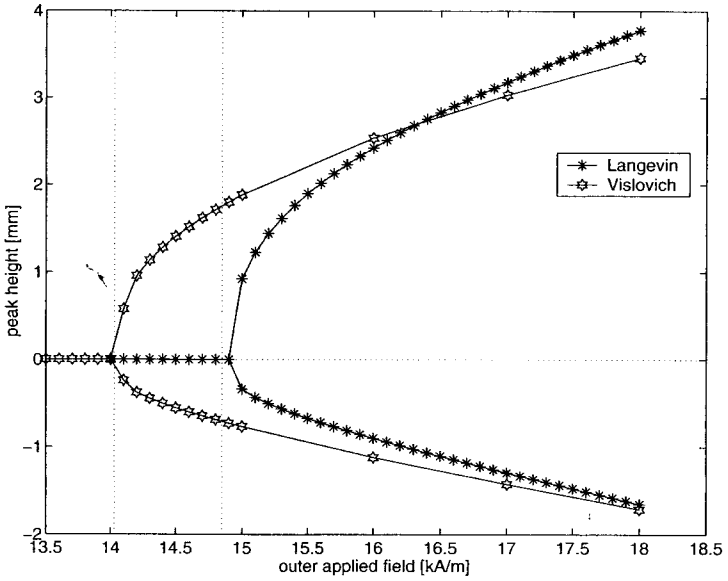

Fig. 13. Comparison of Langevin function and Vislovich approximation

Acknowledgement

For supporting partially the research presented in this paper, the authors like to thanks the German Research Foundation (DFG) under grants within the research group FOR 301 and within the high priority research program SPP 1104, as well as the German Academic Exchange Service (DAAD) and the State Sachsen-Anhalt. Several pictures were produced using the visualisation package GRAPE which was developed at the universities of Bonn and Freiburg i.Br. by the SFB 256 of the DFG.

References

1. Auernhammer, G. K., Brand, H. R.: Thermal convection in a rotating layer of a magnetic fluid. Eur. Phys. J. B **16** (2000) 157–168
2. Bänsch, E., Höhn, B.: Numerical treatment of the Navier-Stokes equations with slip boundary condition. SIAM J. Sci. Comp. **20** (2000) 2144–2162
3. Berkovsky, B. M., Bashtovoy, V.: Magnetic Fluids and Applications Handbook. Begell house, Inc., New York, Wallingford (UK), 1996
4. Cowley, M. D., Rosensweig, R. E.: The interfacial stability of a ferromagnetic fluid. J. Fluid Mech. **30** (1967) 671–688

5. Friedrichs, R., Engel, A.: Pattern and wavenumber selection in magnetic fluids. Phys. Rev. E **64** (2001) 021406
6. Gailitis, A.: Formation of hexagonal pattern on the surface of a ferromagnetic fluid in an applied magnetic field. J. Fluid Mech. **82** (1977) 401–413
7. Girault, V., Raviart, P.: Finite element methods for Navier-Stokes equations. Theory and algorithms. Springer-Verlag, Berlin, 1986
8. John, V., Knobloch, P., Matthies, G., Tobiska, L.: Non-nested multi-level solvers for finite element discretizations of mixed problems. Computing **68** (2002) 343–373
9. John, V., Matthies, G.: MooNMD - a program package based on mapped finite element methods. Technical Report 02-01, Fakultät für Mathematik, Otto-von-Guericke-Universität Magdeburg (2002)
10. Matthies, G.: Finite element methods for free boundary value problems with capillary surface. Shaker Verlag, Aachen, 2002, PhD thesis, Otto-von-Guericke-Universität Magdeburg
11. Matthies, G., Tobiska, L.: Simulation of free surfaces of magnetic liquids. In: Algoritmy 2000, 15th Conf. Scientific Comput., ed. by Handlovičová, A., et. all, Slovak Technical University, Bratislava (2000) 1–10
12. Mitkova, T.: Lösbarkeit eines mathematischen Modells für Dichtungen mit magnetischen Flüssigkeiten. Technische Mechanik **20** (2000) 283–293
13. Odenbach, S.: Magnetoviscous effects in ferrofluids. Lect. Notes Physics, m71, 2002
14. Polevikov, V.: Stability of a static magnetic-fluid seal under the action of an external pressure drop. Fluid Dynamics **32** (1997) 457–461
15. Polevikov, V.: Numerical modelling of equilibrium capillary surfaces: some methods and results. Preprint 98-10, Fakultät für Mathematik, Otto-von-Guericke-Universität Magdeburg (1998)
16. Polevikov, V.: Methods of numerical modeling of equilibrium capillary surfaces. Differents. Uravnenia **35** (1999) 975–981
17. Polevikov, V., Tobiska, L.: Modeling of a dynamic magneto-fluid seal in the presence of a pressure drop. Fluid Dynamics **36** (2001) 890–898
18. Rosensweig, R. E.: Ferrohydrodynamics. Dover Publications, Inc. Mineola, New York, 1997
19. Saad, Y.: Iterative method for sparse linear systems. PWS Publishing Company, 1996
20. Vanka, S.: Block-implicit multigrid calculation of two-dimensional recirculating flows. Comp. Meth. Appl. Mech. Eng. **59** (1986) 29–48

Author Index